Interplay between ATP and hydrolysis free energy in promoting and restraining biochemical switches

Dianjie Li,[1] Siqi Liao,[1] Qi Ouyang,[2] and Fangting Li[1,*]

[1]*School of Physics, Center for Quantitative Biology, Peking University, Beijing 100871, China*

[2]*Department of Physics, Zhejiang University, Hangzhou 310027, Zhejiang Province, China*

(Received 25 February 2024; accepted 10 June 2024; published 11 July 2024)

In living cells, the bistable switches involving phosphorylation-dephosphorylation (PdP) cycles, operate far from thermodynamic equilibrium and consume hydrolysis free energy to perform ultrasensitive response and exhibit strong robustness against noise. Here, we focus on the distinct roles of cellular ATP levels ([ATP]) and hydrolysis free energy ($\Delta\mu$) in bistable switches with different structures of reaction network. Specifically, we herein propose thermodynamically consistent models of single- and double-PdP-cycle bistable switches to study the relationship between network structures and the interplay between [ATP] and $\Delta\mu$. We demonstrate that [ATP] and $\Delta\mu$ act cooperatively to promote the activation of switches in identical networks wherein all phosphorylations promote target production, irrespective of different feedback mechanisms. On the other hand, the competition between [ATP] and $\Delta\mu$ found in the nonidentical, or reversed, networks can enhance the robustness of bistability. We also discuss special network structures inducing multistability or nonmonotonic functions of $\Delta\mu$. Our results gain insight into the relationship between network structures and the roles of [ATP] and $\Delta\mu$ in bistable switches, potentially guiding the future design of synthetic biochemical switches.

DOI: 10.1103/PhysRevResearch.6.033050

I. INTRODUCTION

Living cells are open systems that constantly exchange substances and energy with external environments, thereby maintaining a state far from thermodynamic equilibrium [1–3]. Theoretical studies have investigated the quantitative relationship between biological functions and nonequilibrium conditions, i.e., either free-energy state or dissipation rate [4–12]. For instance, hydrolysis free energy has a critical impact on reducing errors in biosynthetic processes [4], and energy dissipation is essential for enhancing sensing accuracy [9] and synchronization of molecular oscillators [7,8]. Recent experiments highlight the critical role of ATP, the energy-carrying molecule, in different biological processes including protein aggregation [13,14], immune cell response [15], insulin secretion [16,17], and cell cycle control [18]. Specifically, cells depend on ATP hydrolysis free energy provided by reactions of phosphorylation-dephosphorylation (PdP) cycles, to build biochemical and bistable switches with two stable steady states and hysteresis behavior [19]. Since bistability provides ultrasensitive response and reduces input noise, the bistable switch plays a key role in signal transduction and cell cycle control [20–25]. Several studies have demonstrated the impact of hydrolysis free energy on enhancing the robustness and ultrasensitivity of bistable switches [5,19,26–29].

The ATP hydrolysis free energy is $\Delta\mu \sim \ln\{K_{\rm eq}[\mathrm{ATP}]/([\mathrm{ADP}][\mathrm{Pi}])\}$, where the equilibrium constant $K_{\rm eq}$ is 4×10^5 mol/L [19]. The level of $\Delta\mu$ is determined by the concentrations of adenosine triphosphate ([ATP]), adenosine diphosphate ([ADP]), and inorganic phosphate ([Pi]). With the assumption that [Pi] is fixed for simplicity, $\Delta\mu$ depends only on the [ATP]/[ADP] ratio. Accordingly, [ATP] and [ADP] (or $\Delta\mu \sim$ [ATP]/[ADP]) are two parameters that can affect the behaviors of the reaction network containing PdP cycles. Despite the studies investigating the effects of $\Delta\mu$ on various biological functions [4–12], the role of ATP kinetics ([ATP]) and the interplay between [ATP] and ATP thermodynamics ($\Delta\mu$) in the context of biological processes and functions, especially in bistable switches, remain to be elucidated.

Previous studies have reported distinct roles of [ATP] and $\Delta\mu$ in bistable switches controlling two important processes of the yeast cell cycle [18,28]. In DNA replication checkpoints of budding yeast, DNA damage stress turns on the bistable switch of kinase Rad53 to activate the DNA repair pathway [25]. This bistable switch is regulated by a single-PdP-cycle network [Fig. 1(a)]. Theoretical studies have revealed that the bistable switch requires certain levels of $\Delta\mu$, whereby increasing $\Delta\mu$ reduces the thresholds for [ATP] to turn on/off the switch [28]. Such operational control results in a bistable region with two negative slope borders in [ATP] $-$ $\Delta\mu$ space [Figs. 1(b) and 1(c)], suggesting that $\Delta\mu$ and [ATP] cooperate in turning on/off the switches. In contrast, [ATP] and $\Delta\mu$ compete against each other to turn on the bistable switch controlling G2-M transition of fission

*Contact author: lft@pku.edu.cn

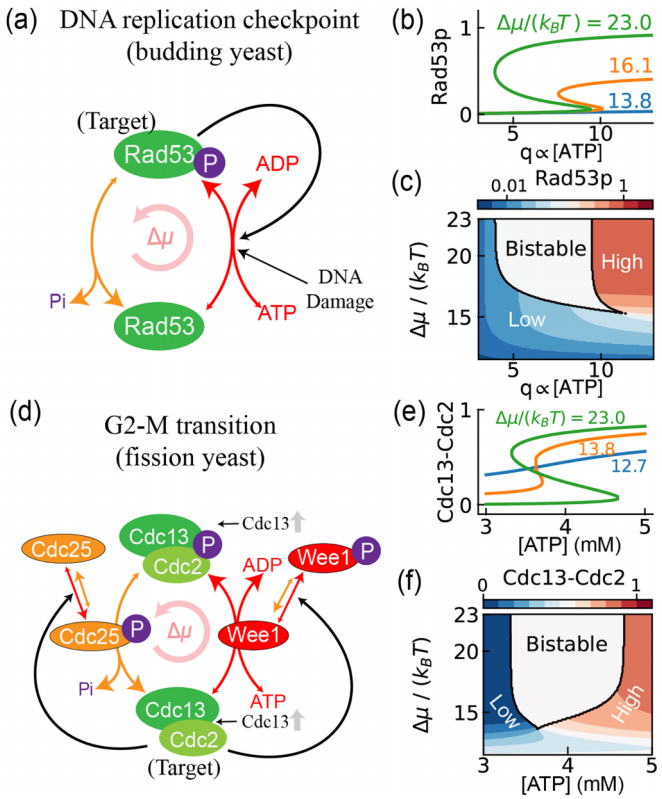

FIG. 1. Phosphorylation-dephosphorylation (PdP) cycle networks and bistability in DNA replication checkpoint and G2-M transition. (a)–(c) Reaction networks (a), bifurcation analysis (b), and [ATP]-$\Delta\mu$ phase diagram (c) of DNA replication checkpoint pathway in budding yeast [28]. DNA damage promotes phosphorylation of the key kinase Rad53. Phosphorylated kinase Rad53p then activates the downstream DNA repair pathway, including the autophosphorylation of Rad53p. $\Delta\mu$ represents the ATP hydrolysis free energy as the driving force of the PdP cycle. (b), (c) The concentration of Rad53p is normalized, and the parameter q is defined in Sec. I of the Supplemental Material (SM) [32]. (d)–(f) Multiple feedback loops governing G2-M transition in fission yeast [18] with bifurcation analysis (e) and [ATP]-$\Delta\mu$ phase diagram (f) of G2-M transition network. Key complex Cdc13-Cdc2 is activated by Cdc25p through dephosphorylation and inactivated by Wee1. Cdc13-Cdc2 promotes phosphorylation of Cdc25 and Wee1. During G2-M transition, elevated cyclin (Cdc13) level promotes the activation of Cdc13-Cdc2 complex. (e), (f) The concentration of Cdc13-Cdc2 is normalized, and the unit of [ATP] is mM (=mmol/L). Red and orange arrows in (a) and (d) are phosphorylation and dephosphorylation reactions. Solid lines in (b) and (e) represent the steady state of target concentration as a function of cellular ATP level. Colored areas in (c) and (f) are monostable. Details of models and parameters are listed in Sec. I of the SM [32].

yeast [Figs. 1(d)–1(f)] [18]. In this case, increasing $\Delta\mu$ can elevate, not reduce, the threshold for [ATP] to turn on the switch. Moreover, the conserved G2-M transition networks in mammalian cells were previously found to be controlled by bistable switches, and, hence, may have the same dependence on [ATP] and $\Delta\mu$ [20,30]. Notwithstanding evidence provided by previous research, we must still ask (1) why ATP kinetics and thermodynamics play distinct roles in different bistable switches, (2) what determines their roles, and (3) whether or not [ATP] and $\Delta\mu$ perform more complicated functions.

To address these questions, we herein propose thermodynamically consistent models of single-PdP-cycle and double-PdP-cycle networks with bistability, and utilize [ATP] $-$ $\Delta\mu$ phase diagrams to investigate how network structures affect the interplay between [ATP] and $\Delta\mu$ in bistable switches. Theoretical and numerical analyses reveal the cooperation between [ATP] and $\Delta\mu$ in turning on/off switches with identical network structures wherein all phosphorylation reactions promote target production. In reversed, or nonidentical networks, [ATP] may, however, compete against $\Delta\mu$ to turn on/off the switch. In this instance, competition could enhance the robustness of bistability against ATP fluctuation. Additionally, we discuss tristability and nonmonotonic effects of $\Delta\mu$ on the bistablity found in the reversed networks.

II. MODELS

A. Single phosphorylation-dephosphorylation cycle system as bistable switch

Generic reactions of a PdP cycle can be written as

$$\begin{aligned} \mathrm{ATP} + S &\underset{\mathrm{k_{s,p-}\ F}}{\overset{\mathrm{k_{s,p}\ F}}{\rightleftharpoons}} \mathrm{ADP} + S_p \\ S_p &\underset{\mathrm{k_{s,dp-}\ G}}{\overset{\mathrm{k_{s,dp}\ G}}{\rightleftharpoons}} S + \mathrm{Pi}, \end{aligned} \tag{1}$$

where S_p is the phosphorylated molecular S assumed to be the target product; F and G are the catalysts of PdP cycle and contain input signals and self-feedback of S_p or S; and $k_{s,p}$, $k_{s,p-}$, $k_{s,dp}$, and $k_{s,dp-}$ are the reaction constants.

Assuming that total concentration of molecule S is a constant ($[S_T] = [S] + [Sp]$), the ordinary differential equation of target product concentration is written as

$$\begin{aligned} \frac{d[S_p]}{dt} &= (J_p + J_{dp-}) - (J_{p-} + J_{dp}) \\ &= (k_{s,p}[\mathrm{ATP}]F + k_{s,dp-}[\mathrm{Pi}]G)([S_T] - [S_p]) \\ &\quad - (k_{s,p-}[\mathrm{ADP}]F + k_{s,dp}G)[S_p]. \end{aligned} \tag{2}$$

The free energy provided by the hydrolysis of one molecule ATP is defined as [19]

$$\begin{aligned} \Delta\mu &= \Delta\mu_0 + k_B T \ln \frac{[\mathrm{ATP}]}{[\mathrm{ADP}][\mathrm{Pi}]} \\ &= k_B T \ln \frac{k_{s,p}k_{s,dp}[\mathrm{ATP}]}{k_{s,p-}k_{s,dp-}[\mathrm{ADP}][\mathrm{Pi}]} \\ &= k_B T \ln \frac{J_p J_{dp}}{J_{p-} J_{dp-}}, \end{aligned} \tag{3}$$

where $[X]$ is the concentration of molecule $X \in$ {ATP, ADP, Pi} and the equilibrium constant is

$$K_{\mathrm{eq}} = e^{\Delta\mu_0/(k_B T)} = \frac{k_{s,p}k_{s,dp}}{k_{s,p-}k_{s,dp-}} = 4.9 \times 10^5\ \mathrm{mol/L}. \tag{4}$$

When $\Delta\mu = 0$, the system reaches a state of thermodynamic equilibrium. However, the system is far from equilibrium at

the physiological state $\Delta\mu_{\rm phys} \approx 23\ k_BT$, where k_B is the Boltzmann constant and T is the temperature [19].

By introducing one positive feedback through F or G, the system may perform bistable behaviors. For example, both the Schlögl model, a canonical example of a chemical reaction system that exhibits bistability [27,29,31], and the PdP cycle of Rad53 [25,28] involve the autocatalysis of S_p by its dimer ($F = [S_p]^2 I$ and $G = I$). Assuming that $[S_p] = x$, $[S_T] = 1$, $k_{s,p}[\mathrm{ATP}] = a$, $k_{s,p-}[\mathrm{ADP}] = d$, $k_{s,dp} = p_1$, $k_{s,dp-}[\mathrm{Pi}] = p_2$, and input signal $I = 1$, we simplify Eq. (2) as

$$\frac{dx}{dt} = -(a+d)x^3 + ax^2 - (p_1+p_2)x + p_2, \tag{5}$$

where $\Delta\mu = k_BT\ln[p_1a/(p_2d)]$. Other feedback mechanisms of single-PdP-cycle network are discussed in Sec. II of the Supplemental Material (SM) [32].

B. Double-PdP-cycle systems with bistability and different network structures

The reactions of the double-PdP-cycle network can be written as

$$\begin{aligned}
\mathrm{ATP} + S &\underset{k_{s,p-}\ F_s}{\overset{k_{s,p}\ F_s}{\rightleftharpoons}} \mathrm{ADP} + S_p,\\
S_p &\underset{k_{s,dp-}\ G_s}{\overset{k_{s,dp}\ G_s}{\rightleftharpoons}} S + \mathrm{Pi},\\
\mathrm{ATP} + Y &\underset{k_{y,p-}\ F_y}{\overset{k_{y,p}\ F_y}{\rightleftharpoons}} \mathrm{ADP} + Y_p,\\
Y_p &\underset{k_{y,dp-}\ G_y}{\overset{k_{y,dp}\ G_y}{\rightleftharpoons}} Y + \mathrm{Pi},
\end{aligned} \tag{6}$$

where S_p is the target product of the network, and F_s and G_s are the catalysts in the PdP cycle of S_p, which may contain input signals, self-feedback of S_p or S, and regulation of Y or Y_p. Similarly, in PdP cycle reactions of molecule Y, F_y and G_y are catalysts involving input signals and the regulation terms of S_p or S; $k_{i,p}$, $k_{i,p-}$, $k_{i,dp}$, and $k_{i,dp-}$ are the reaction constants in the PdP cycle reactions of molecular $i = Y, S$, which are constrained by the equilibrium condition Eq. (4).

The equations for $[S_P]$ and $[Y_P]$ are written as

$$\begin{aligned}
\frac{d[S_p]}{dt} &= (k_{s,p}[\mathrm{ATP}]F_s + k_{s,dp-}[\mathrm{Pi}]G_s)([S_T] - [S_p])\\
&\quad - (k_{s,p-}[\mathrm{ADP}]F_s + k_{s,dp}G_s)[S_p],\\
\frac{d[Y_p]}{dt} &= (k_{y,p}[\mathrm{ATP}]F_y + k_{y,dp-}[\mathrm{Pi}]G_y)([Y_T] - [Y_p])\\
&\quad - (k_{y,p-}[\mathrm{ADP}]F_y + k_{y,dp}G_y)[Y_p].
\end{aligned} \tag{7}$$

The network structure is determined by F_i and G_i ($i = s, y$) as

$$\begin{aligned}
F_i &= I_i^{(f)} \prod_{j=s,y} [\alpha_{i,j}g_{j,p} + (1-\alpha_{i,j})g_j]^{\theta_{i,j}\beta_{i,j}},\\
G_i &= I_i^{(g)} \prod_{j=s,y} [\alpha_{i,j}g_{j,p} + (1-\alpha_{i,j})g_j]^{\theta_{i,j}(1-\beta_{i,j})},
\end{aligned}$$

where $\theta_{i,j}$ indicates whether molecule i's PdP cycle reaction is regulated by molecule j ($\theta_{i,j} = 1$) or not ($\theta_{i,j} = 0$); $\beta_{i,j} \in \{1, 0\}$ denotes whether the regulation through F_i ($\beta_{i,j} = 1$) or G_i; and $\alpha_{i,j} \in \{1, 0\}$ signifies whether molecule i is regulated by phosphorylated molecule j ($\alpha_{i,j} = 1$) or the dephosphorylated molecule.

Since the target product is S_p, we assume that the regulation term of S_p is $g_{s,p} = [S_p]^2$ and Y_p or Y cannot regulate itself ($\alpha_{y,s} = \alpha_{s,s} = 1$ and $\theta_{y,y} = 0$), similar to the single-PdP-cycle system. Regulation by Y is linear, i.e., $g_{y,p} = [Y_p]$, and $g_y = [Y_T] - [Y_p]$. The total concentrations for each molecule are constants, where $[X_T] = [X] + [X_p]$ ($X = S, Y$). Input signals are set as $I_i^{(f)} = I_i^{(g)} = 1$ for simplicity. The hydrolysis free energy $\Delta\mu$ is a global parameter for these PdP cycles [Eq. (3)], since the rate constants (k) of each PdP cycle satisfy the same equilibrium condition [Eq. (4)].

III. RESULTS

In the following sections, we discuss the cooperation between [ATP] and $\Delta\mu$ in single-PdP-cycle switches (Sec. III A), the relationship between network structures and [ATP]-$\Delta\mu$ interplay in double-PdP-cycle switches (Sec. III B), the robustness of bistability against [ATP] and $\Delta\mu$ fluctuations (Sec. III C), and complex roles of $\Delta\mu$ in bistable switches (Sec. III D).

A. ATP concentration and hydrolysis free energy cooperatively turn on/off the single-PdP-cycle bistable switch

We first discuss the roles of ATP concentration ([ATP]) and hydrolysis free energy ($\Delta\mu$) in the single-PdP-cycle system [Eq. (1)]. As shown in Fig. 1, the slopes of bistable region borders in $[\mathrm{ATP}] - \Delta\mu$ phase diagram characterize their roles. For example, in Fig. 1(c), increasing [ATP] and $\Delta\mu$ simultaneously can turn on the switch when the slope of the right border is negative. However, Fig. 1(f) shows the right border with positive slope, indicating that an increase in $\Delta\mu$ results in the requirement of a higher threshold of [ATP] to turn on the switch.

Bistable region borders in the $[\mathrm{ATP}] - \Delta\mu$ phase diagram are groups of saddle-node bifurcation points. Assuming [Pi] as a constant, the function $f_s = d[S_p]/dt$ on these points ([ATP]*, [ADP]*, $[S_p]^*$) satisfy the two following conditions [33]:

$$f_s([\mathrm{ATP}]^*, [\mathrm{ADP}]^*, [S_p]^*) = 0, \quad \left.\frac{\partial f_s}{\partial [S_p]}\right|_{[S_p]^*} = 0. \tag{8}$$

Considering the total differential of f_s, we have

$$\Delta f_s = \frac{\partial f_s}{\partial [\mathrm{ATP}]}\Delta[\mathrm{ATP}] + \frac{\partial f_s}{\partial [\mathrm{ADP}]}\Delta[\mathrm{ADP}] + \frac{\partial f_s}{\partial [S_p]}\Delta S_p$$

Substituting the conditions [Eqs. (8)], we have

$$\frac{d[\mathrm{ADP}]}{d[\mathrm{ATP}]} = -\frac{\partial f_s/\partial[\mathrm{ATP}]}{\partial f_s/\partial[\mathrm{ADP}]}$$

The slope of borders (SLP) in $[\mathrm{ATP}] - \Delta\mu$ space can be derived by using the definition of $\Delta\mu$ in Eq. (3) as

$$\begin{aligned}
\mathrm{SLP} &\sim \frac{1}{[\mathrm{ATP}]} - \frac{1}{[\mathrm{ADP}]}\frac{d[\mathrm{ADP}]}{d[\mathrm{ATP}]}\\
&= \frac{[\mathrm{ATP}]\partial f_s/\partial[\mathrm{ATP}] + [\mathrm{ADP}]\partial f_s/\partial[\mathrm{ADP}]}{[\mathrm{ATP}][\mathrm{ADP}]\partial f_s/\partial[\mathrm{ADP}]}.
\end{aligned} \tag{9}$$

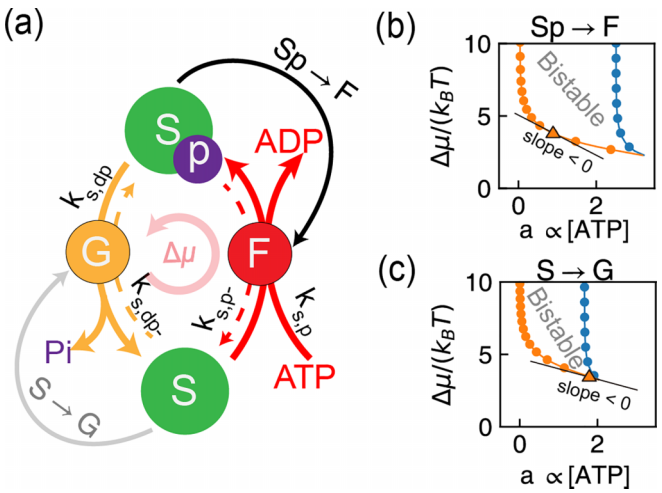

FIG. 2. Single-PdP-cycle networks and bistable regions. (a) Schematics of single-PdP-cycle bistable switches with different positive feedback mechanisms ($Sp \to F$ or $S \to G$). (b), (c) Examples of bistable region borders in $[\mathrm{ATP}] - \Delta\mu$ space with different feedback mechanisms, where $a = k_{s,p}[\mathrm{ATP}]$. The bistable region was first computed in the a and $d = k_{s,p-}[\mathrm{ADP}]$ space, and showed in the $a - \Delta\mu$ space. (b) Network with feedback ($Sp \to F$), $p_1 = 10^{-2}$ and $p_2 = 10^{-5}$. (c) Network with feedback ($S \to G$), $p_1 = 10$ and $p_2 = 5$.

In the single-PdP-cycle system [Eqs. (1) and (2)], we have

$$\frac{\partial F}{\partial[\mathrm{ATP}]} = \frac{\partial F}{\partial[\mathrm{ADP}]} = \frac{\partial G}{\partial[\mathrm{ATP}]} = \frac{\partial G}{\partial[\mathrm{ADP}]} = 0$$

and

$$\frac{\partial f_s}{\partial[\mathrm{ATP}]} = k_{s,p}F([S_T] - [S_P]^*),$$
$$\frac{\partial f_s}{\partial[\mathrm{ADP}]} = -k_{s,p-}F[S_P]^*$$

on the bistable region borders ($[S_P] = [S_P]^*$). Therefore, the slope of borders is formulated as

$$\mathrm{SLP} \sim \frac{k_{s,p-}F[\mathrm{ADP}][S_P]^* - k_{s,p}F[\mathrm{ATP}]([S_T] - [S_P]^*)}{[\mathrm{ATP}][\mathrm{ADP}]k_{s,p-}F[S_P]^*},$$

where the denominator of SLP is positive and the numerator of SLP is $(J_{p-} - J_p)$. At physiological steady states ($d[S_p]/dt = 0$), the system consumes hydrolysis free energy ($\Delta\mu > 0$), requiring $J_p > J_{p-}$. Consequently, in the single-PdP-cycle system, the signs of bistable border slopes in $[\mathrm{ATP}] - \Delta\mu$ space are negative when $\Delta\mu > 0$ and independent of network structures (F and G).

Next, we investigate the influence of different feedback mechanisms in the single-PdP-cycle system. For simplicity, we discuss the networks with only one positive feedback regulation: (1) $\mathrm{F} = [S_p]^2$, (2) $G = [S]^2$, (3) $F = [S]^2$, and (4) $G = [S_p]^2$, as shown in Fig. S1(a) [32]. For the network with $F = [S_p]^2$, $G = 1$, we derive the border functions $d_{1/2}(a)$ in the Appendix, and the slopes of both borders are proved analytically to be negative, which is validated by numerical simulations with randomly sampled parameter sets (p_1 and p_2), as shown in Figs. 2(b), S1(d), and S1(e) [32]. For the networks with $F = 1$, $G = [S]^2$, we also sample the parameters (p_1 and p_2) and calculate the slopes of both borders under different $\Delta\mu$ levels. The sampling results confirm that all the slopes are negative [Figs. 2(c) and S1(e)] [32]. However, the other two networks $F = 1, G = [S_p]^2$ and $F = [S]^2, G = 1$ show no bistability under $\Delta\mu > 0$, since they require that the PdP cycles operate in the revere direction ($\Delta\mu < 0$) to form positive feedback, and thus exhibit bistability [Fig. S1(b)] [32].

Therefore, based on the analytical analysis of SLP [Eq. (9)] and numerical results of the single-PdP-cycle networks with different feedback mechanisms (Figs. 2 and S1) [32], we find that the slopes of bistable region borders of single-PdP-cycle switches are negative under $\Delta\mu > 0$, irrespective of the network structures. These results suggest that [ATP] and $\Delta\mu$ cooperatively turn on/off the single-PdP-cycle bistable switch.

B. Phosphorylation contribution to target molecules determines the interplay between $\Delta\mu$ and ATP level in bistable switches: cooperation or competition

In this section, we discuss the interplay between the ATP level and $\Delta\mu$ in double-PdP-cycle switches. Based on the assumptions made in Sec. II B, we have 20 different network structures for a double-PdP-cycle system, and 16 of them could exhibit bistability, termed Network 0 to Network 15 [Figs. 3(c) and S2] [32]. We classify these networks into two types: identical and reversed networks, based on the structure factor, phosphorylation contribution to target molecules (PC). PC is defined as the ratios of phosphorylation reactions that promote target molecule production. The network with PC = 1 is termed the identical network, because all phosphorylations in the network have the same contribution. The reversed network is defined as the network with PC < 1, where at least one of the phosphorylations reduces target molecules. There are only two phosphorylations in double-PdP-cycle networks and the phosphorylation of S always promotes the target S_p production, thus PC is determined by the contribution of phosphorylation of Y. For example, Fig. 3(a) shows that Network 12 is an identical network with PC=(1+1)/2=1 because phosphorylation of molecule Y produces more Y_p, Y_p then catalyzes the phosphorylation from S to target S_p, and thus phosphorylation of Y promotes the target production. However, in Network 13 (reversed), Y_p enhances the dephosphorylation and, hence, reduction of S_p, indicating that only the phosphorylation reaction of S contributes positively to the target S_p (PC=1/2=0.5). Apart from PC, we introduce another index to characterize the network structure. This index is termed the positive feedback level (PFL), which is defined as the sum of feedback array. The feedback array represents the types of all the feedback regulations in the network, e.g., $[-1, 1]$ means one negative and one positive feedback for S_p (PFL=−1+1=0).

Applying the analytical method described in Sec. III of the SM [32], we prove that both slopes of bistable region borders are negative for identical networks. Hence, for all identical double-PdP-cycle networks (PC = 1), $\Delta\mu$ and the ATP level always cooperate to turn on/off switches as those found in single-PdP-cycle networks. The conclusion remains valid in the identical network even with more upstream PdP cycles

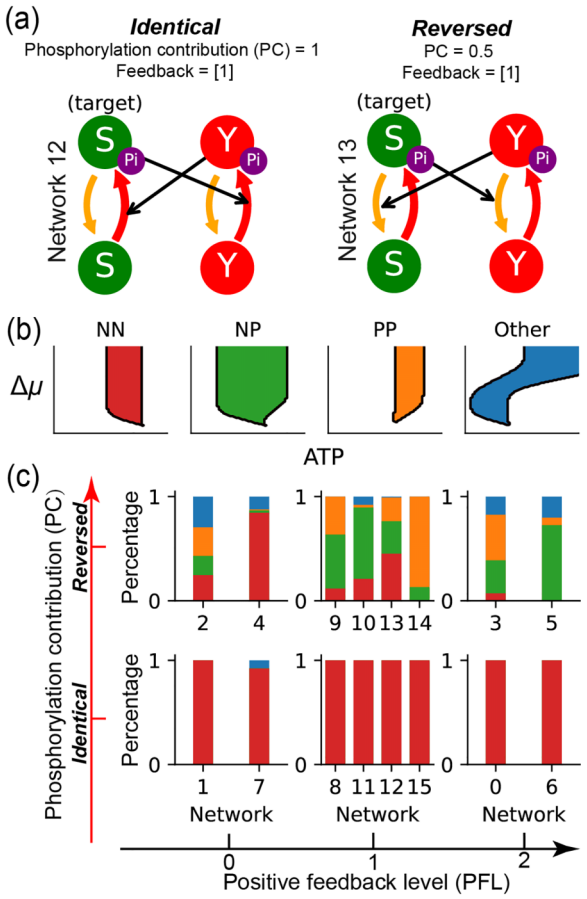

FIG. 3. Double-PdP-cycle networks and corresponding bistable area types. (a) Examples of identical and reversed double-PdP-cycle networks. Phosphorylation contribution (PC) quantifies the ratio of phosphorylation reaction that contributed positively to the target. Feedback is the array of all feedback signs. (b) Examples of four bistable region types in the [ATP] − $\Delta\mu$ phase diagram. The white region is monostable and the colored region is bistable. In these diagrams, the x axis is [ATP] and the y axis is $\Delta\mu \sim$ [ATP]/[ADP]. With a given [ATP], we change [ADP] to modify $\Delta\mu$. (c) Percentages of bistable region types in parameter sampling results of different networks. Networks are clustered according to two structure indexes, PC and positive feedback level (PFL).

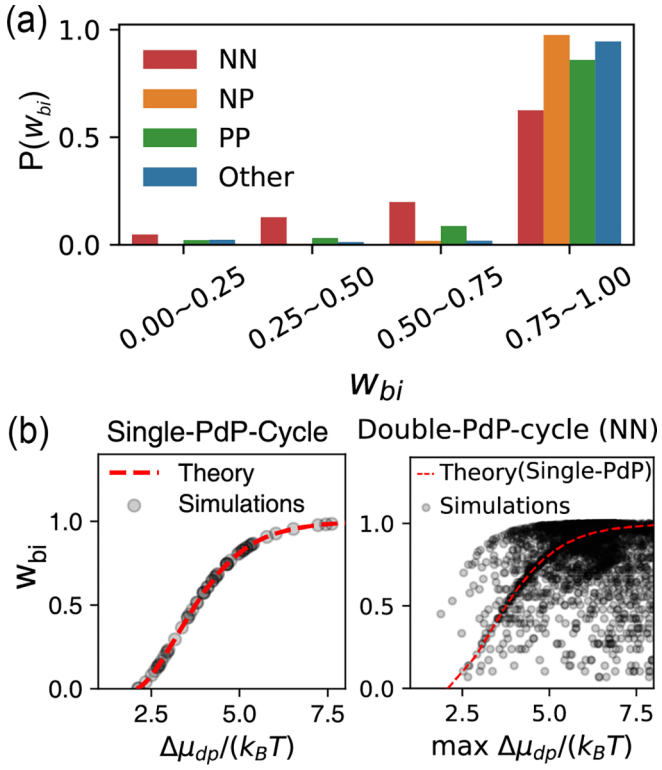

FIG. 4. Relative width of bistable region ($w_{\rm bi}$) in different bistable types. (a) Relative frequency $P(w_{\rm bi})$ of $w_{\rm bi}$ in different bistable types, based on the sampling results of double-PdP-cycle switches. (b) Dephosphorylation energy ($\Delta\mu_{dp}$) bounds the width of NN bistable region in PdP-cycle switches. The width is calculated with $\Delta\mu \to$ inf in the single-PdP-cycle networks ($S_p \to F$) and $\Delta\mu \sim 23\ k_BT$ in the double-PdP-cycle networks.

(Sec. III of the SM [32]). In contrast, the border slopes in reversed networks have various choices [Figs. 3(b) and 3(c)], for instance, one positive and one negative slope or both positive slopes of borders, which depends on the parameters.

Therefore, we use numerical simulations to validate the analytical results and investigate different roles of $\Delta\mu$ and ATP level in reversed networks. For each network structure, the parameters $k_{i,p}$, $k_{i,p-}$, and $k_{i,dp}$ are randomly sampled, where $i \in s, y$. $k_{i,dp-}$ is calculated by thermodynamic constraint [Eq. (4)], while the bistable region is computed in [ATP] − $\Delta\mu$ space. We classify these bistable region shapes into four types according to the signs of the border slopes: negative-negative (NN), negative-positive (NP), positive-positive (PP), and other, as shown in Fig. 3(b). In NN, NP, and PP, the slopes of borders monotonically change with increased $\Delta\mu$ and become infinite when $\Delta\mu$ is large enough. Other bistable region shapes include slopes as a nonmonotonic function of $\Delta\mu$ or more complex shapes of bistable region, as discussed in Sec. III D.

In Fig. 3(c), the sampling results show that the identical networks only have the NN type of bistable region, except for Network 7. Although Network 7 could induce the NN or other type, the slopes of the other-type bistable region in Network 7 are also negative like those of NN [Fig. 5(f)]. Hence, based on the sampling results of all identical double-PdP-cycle networks with different feedback mechanisms, the slopes of bistable region borders are always negative. Accordingly, $\Delta\mu$ cooperates with [ATP] to turn on/off double-PdP-cycle switches, irrespective of the feedback mechanisms. However, because all types of bistable regions can be found in the sampling results of reversed networks, slopes of borders in reversed networks could be either positive or negative, and depend on the parameters we sampled, as shown in Fig. 3(c). These results suggest that $\Delta\mu$ and [ATP] could either compete or cooperate to turn on/off double-PdP-cycle switches with reversed network structures. In addition, we find that enhanced positive feedback level could increase the ratio of the NP type in sampling results of reversed networks [Fig. 3(c)]. Accordingly, since the G2-M regulation network has two positive feedbacks and the phosphorylation of Cdc13-Cdc2 reduces the target (Cdc13-Cdc2), the G2-M regulation network is a reversed network with a strong positive feedback

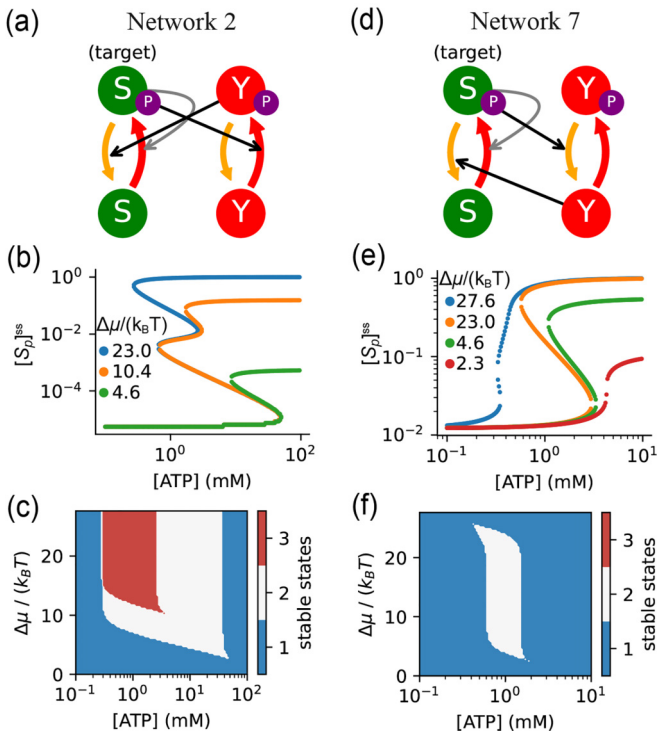

FIG. 5. Multistable states and the nonmonotonic function of $\Delta\mu$ in other types of double-PdP-cycle switches. (a)–(c) Tristability in Network 2. When free energy $\Delta\mu$ elevates, the number of steady state S_p ($[S_p]^{ss}$) changes from three to five (b), thus accounting for the switch change from bistable to tristable (c). (d)–(f) Nonmonotonic effect of $\Delta\mu$ found in Network 7. Increasing $\Delta\mu$ to $2.3k_BT$ first induces bistability and broadens the region width like NN, NP, and PP switches. However, width begins to narrow around $\Delta\mu \sim 20k_BT$, and bistability finally disappears when $\Delta\mu > 27.8k_BT$.

level (PFL=2) and more likely to have the NP-type bistable region [Figs. 1(d)–1(f)].

C. Bistability robustness is strengthened by the opposing roles of cellular $\Delta\mu$ and ATP level (NP) and limited by the dephosphorylation free energy (NN)

In identical networks, hydrolysis free energy $\Delta\mu$ is only consumed for producing target molecules, whereas part of hydrolysis free energy is used to inhibit target production in reversed networks. We ask why cells apply inefficient networks (reversed) in some cellular processes. Based on bistable shapes, $\Delta\mu$ and [ATP] have an opposing effect on bistable switches with NP types, since increased $\Delta\mu$ can elevate the "on" thresholds for [ATP]. This then prompted us to ask why some bistable switches have opposing roles of $\Delta\mu$ and [ATP] in NP types. Owing to the fluctuations of ATP concentration and $\Delta\mu$ in cells [14,34–37], we proposed that cells choose the inefficient reversed network with NP-type bistable regions to maintain the robustness of bistable switches by countering these fluctuations. In this section, we discuss how bistable types and dephosphorylation energy affect the robustness of bistability against these fluctuations.

When the bistable region is NN type, the system could easily move out of the bistable region since $\Delta\mu \sim$ [ATP]/[ADP] and [ATP] generally change in the same direction, i.e., from left bottom to right up, and cooperate to turn on/off the switch. However, when the region is NP type, two different signs of slopes can broaden the width of the bistable region by increasing $\Delta\mu$. Hence, an intuitive guess is that robustness against these fluctuations in NN is probably lower than that in NP. Therefore, we perform simulations to demonstrate that the opposing roles of $\Delta\mu$ and [ATP] in NP types contributes to a wider bistable region under physiological conditions and a larger size of the bistable region in [ATP] $-$ $\Delta\mu$ space, which enhance the robustness of bistable switches against [ATP] and $\Delta\mu$ fluctuations.

First, to confirm the relationship between robustness and bistable types, we quantify the robustness of bistable switches by the relative width of bistable region [5,29] as

$$w_{\rm bi} = \frac{[\mathrm{ATP}]_+ - [\mathrm{ATP}]_-}{[\mathrm{ATP}]_+ + [\mathrm{ATP}]_-}, \tag{10}$$

where $[\mathrm{ATP}]_+$ and $[\mathrm{ATP}]_-$ represent [ATP] of left and right bistable borders with a given $\Delta\mu$. Next, we calculate $w_{\rm bi}$ in the sampling results of double-PdP-cycle under $\Delta\mu_{\rm phys}$ and compute the distribution of $w_{\rm bi}$ in different bistable types [Fig. 4(a)]. NP shows the highest relative frequency of $w_{\rm bi} \in [0.75, 1]$ among all four types, and more than 80% of the samples in PP and other lie in $w_{\rm bi} \in [0.75, 1]$, as well. In contrast, 40% of $w_{\rm bi}$ in NN types are less than 0.75. Hence, among four bistable region types, the bistable switch with the NP type is most likely to have a wide bistable region under physiological condition.

Second, we quantify the robustness of bistable switches by the size of the bistable region in [ATP] $-$ $\Delta\mu$ space (Sec. IV of the SM and Fig. S4 [32]). We use the sampling result of Network 2, wherein the distribution of bistable region types is nearly uniform. For each parameter set sampled in Network 2, we change one parameter and compute the new bistable region to examine whether the shape of bistable region is transformed into another type [Fig. S4(a)] [32]. By applying such parameter perturbations, we find that transforming the bistable region to the NP type is most likely to increase the size [Fig. S4(b)] [32]. Therefore, we conclude that, in comparison with the cooperation between [ATP] and $\Delta\mu$ (NN types), the opposing role of $\Delta\mu$ and [ATP] (NP types) has higher probability to enhance the robustness of bistablity in double-PdP-cycle networks.

Apart from the relationship between the bistable type and bistability robustness, we also find that dephosphorylation reactions can affect robustness. In single-PdP-cycle bistable switches with feedback ($S_p \to F_s$), we derive the analytical expression of $w_{\rm bi}$ by substituting $d(a)$ into Eq. (10) with $d = 0$ ($\Delta\mu \gg 0$) as

$$\max\{w_{\rm bi}\} = \frac{\sqrt{\frac{p_1}{p_2}\left(\frac{p_1}{p_2} - 8\right)^3}}{\left(\frac{p_1}{p_2}\right)^2 + 20\frac{p_1}{p_2} - 8}. \tag{11}$$

This equation suggests that $\frac{p_1}{p_2}$ bounds the maximum width of the bistable region, and bistable switches work only when $p_1/p_2 > 8$. Notably, $\Delta\mu$ can be divided into two terms, as

follows:

$$\frac{\Delta\mu}{k_BT} = \frac{\Delta\mu_p + \Delta\mu_{dp}}{k_BT} = \ln\left(\frac{a}{d}\right) + \ln\left(\frac{p_1}{p_2}\right). \quad (12)$$

Thus, Eq. (11) indicates that the level of dephosphorylation free energy, as represented by $\Delta\mu_{dp} = k_BT\ln(p_1/p_2)$, bounds the robustness of bistability in single-PdP-cycle networks ($S_p \to F_s$), as shown in Fig. 4(b). In NN-type sampling results of double-PdP-cycle switches, we observed a similar bound on $w_{\rm bi}$ by maximum $\Delta\mu_{dp}$ of S_p and Y_p cycles, even though this bound is looser than that in single-PdP-cycle switches [Fig. 4(b)]. Intriguingly, a group of NN double-PdP-cycle switches follows the bound in single-PdP-cycle, which may result from weak impact of Y_p, causing, in turn, the switch to become single-PdP-cycle-like. No obvious bound by $\Delta\mu_{dp}$ is found in NP, PP, and other types of double-PdP-cycle switches (Fig. S3) [32].

D. Network structures and feedback mechanisms associate with multistability and complex roles of $\Delta\mu$ in double-PdP-cycle switches

Finally, we explore some interesting shapes of the bistable region in other types. Apart from one positive feedback to sustain bistability, several structures of double-PdP-cycle networks involve another positive/negative feedback (Fig. S2) [32]. These feedbacks and specific network structures could result in distinct phase diagrams in the [ATP] $-$ $\Delta\mu$ space.

In Fig. 5(a), Network 2 has one positive feedback from S_p to its phosphorylation, and one negative feedback from S_p to phosphorylation of $Y \leftarrow Y_p$ (Y_p as phosphatase for S_p). Some sample parameters of Network 2 show tristable behaviors. In Fig. 5(b), for example, three steady states of $[S_p]$ can be observed under low $\Delta\mu(= 4.6\ k_BT)$ and high [ATP] range. When $\Delta\mu$ increases to $10\ k_BT$, two more steady states emerge, providing the possibility of forming tristable switches. Elevating $\Delta\mu$ to a physiological level ($23\ k_BT$) further widens the possible tristable region. These behaviors of $\Delta\mu$ and the system response lead to an intriguing phase diagram in [ATP] $-$ $\Delta\mu$ space, i.e., a NN-type tristable region locates inside an NN-type bistable region [Fig. 5(c)]. Such multistability can also be found in Network 7. These findings suggest that negative feedback through dephosphorylation of S_p is a potential underlying mechanism for multistability in double-PdP-cycle networks.

In the sampling results of Network 7, we found a special bistable region type where $\Delta\mu$ plays a reversed and constraining role in bistability robustness [Figs. 5(d)–5(f)]. In Fig. 5(e), when $\Delta\mu$ increases from $2.3\ k_BT$, the width of the bistable region increases to a fixed level as in the normal NN type, indicating that $\Delta\mu$ can enhance robustness. However, when $\Delta\mu$ is larger than $20\ k_BT$, the bistable region becomes smaller and finally disappears under $\Delta\mu \sim 27.6\ k_BT$. Then, such a sample of Network 7 is characterized by an islandlike bistable region [Fig. 5(f)]. This phenomenon suggests that $\Delta\mu$ around the physiological level ($23\ k_BT$) will constrain the robustness of bistability; in other words, it will engage in role reversal in comparison with NN, NP, and PP types. Another special shape of the bistable region frequently found in other types is characterized by the nonmonotonic change of bistable region width with increasing $\Delta\mu$ [Figs. 3(b) and S5] [32]. All the networks involving such a special bistable region have one regulation from Y to the PdP cycle of S (Networks 4–7, 10, and 11 in Fig. S2) [32].

IV. DISCUSSIONS

This paper demonstrates that the structure of the phosphorylation-dephosphorylation-cycle network determines the functions of [ATP] and $\Delta\mu$ in bistable switches. Our theoretical and numerical results demonstrate that [ATP] and $\Delta\mu$ act cooperatively to turn on/off the switches in identical networks, irrespective of the number of PdP cycles and type of self-feedback mechanisms. Meanwhile, reversed networks show various roles of [ATP] and $\Delta\mu$. We explore the advantage of seemingly inefficient reversed networks and explain why biological processes choose them rather than the more economical identical networks. Although few PdP cycles in reversed networks retrain the switch, this structure likely satisfies various demands of biological processes. For example, the NP-type bistable region can strongly enhance the robustness of bistable switch by increasing $\Delta\mu$ such as exhibited in G2/M transition where the cell cycle must be fairly robust against perturbations. In a contrasting example, the Rad53 system functions to prohibit errors of DNA synthesis and, therefore, needs to be sensitive to the DNA damage signal, a case that requires less robustness of bistability. Consequently, the Rad53 system utilizes the simplest identical network with NN-type bistable region.

Apart from the robustness of bistablility, the [ATP] $-$ $\Delta\mu$ phase diagram also indicates the roles of hydrolysis free energy $\Delta\mu$ in different bistable switches. First, in all of the bistable switches we discuss, the system requires a certain level of $\Delta\mu$ to exhibit bistability, which is characterized by the bottom intersection point ($[\text{ATP}]_c$, $\Delta\mu_c$) of bistable region borders. Generally, $\Delta\mu(\sim\Delta\mu_c)$ could affect the bistable region borders and the bistable switch, and the region is widened with increasing $\Delta\mu$. However, border shapes are insensitive to $\Delta\mu$ under physiological conditions in bistable switches governing the G2-M transition and DNA replication checkpoint, since $\Delta\mu_c \ll \Delta\mu_{\rm phys} \sim 23k_BT$ (Fig. 1). To explain, $\Delta\mu_{\rm phys}$ with fixed [ATP] and [Pi] means that [ADP] is much lower; under these conditions, perturbation around high $\Delta\mu$ (low [ADP]) would not affect reactions in the system. Therefore, it is advantageous that these bistable switches are robust against $\Delta\mu$ noise under physiological condition. Second, the roles of $\Delta\mu$ in the other type of reversed networks are much different, which may shed light on multifunctional design of synthetic biochemical switches. For example, in Network 7, bistable region borders depend on $\Delta\mu$ even under physiological levels and, more interestingly, the bistable region narrows when $\Delta\mu$ increased [Fig. 5(f)]. Based on this special role of $\Delta\mu$, one can add NN-type [Fig. 1(c)] and islandlike [Fig. 5(f)] switches together in the system. Then, one can change the functions of the system only by controlling $\Delta\mu$, e.g., maintaining $\Delta\mu = \Delta\mu_{\rm phys}$ keeps two switches working normally, and elevating $\Delta\mu$ mutes the islandlike switch with no effect on the other. Third, when we divide $\Delta\mu$ into phosphorylation $\Delta\mu_p$ and dephosphorylation $\Delta\mu_{dp}$, we find that $\Delta\mu_{dp}$ has to step over a threshold in single-PdP-cycle networks, as a necessary

condition for the bistability. In some *in vitro* experiments, this hypothesis could be verified, to some extent, by just altering *Pi* concentration. Finally, in other biological processes, not bistable switches, the functional region in [ATP] $-\Delta\mu$ space may become complicated and sensitive to $\Delta\mu$ under physiological condition. For example, in the glucose response pathway of pancreatic β cells, ATP can affect the open rate of the K_{ATP} channel through binding, not hydrolysis, and the response region is S-shaped in [ATP] $-\Delta\mu$ space [38].

This paper, together with our previous studies [18,28], emphasizes that the roles of [ATP] and other $\Delta\mu$-related parameters are important when we are discussing the impact of $\Delta\mu$ on biological functions. Most of the previous research focused on the lower bound or the minimum dissipation rate of the hydrolysis free energy for the biological functions, while they generally ignored the impacts of [ATP] and other parameters [5–12]. In our paper, we have shown that under same thermodynamic condition ($\Delta\mu$), the biochemical network could exhibit different behaviors due to the variations of $\Delta\mu$-related parameters. For example, increasing [ATP] with a constant [ATP]/[ADP] ratio and $\Delta\mu = 23k_BT$ could induce a transition in the Rad53 reaction network from a monostable state to a bistable state, as shown in Fig. 1(b). Meanwhile, the reduction of [Pi] and $\Delta\mu_{dp}$ may decrease the width of the bistable region [Fig. 4(b)].

Limitations of this paper are (1) the general relationship between network structures and phase diagrams for bistability is not examined in more complex networks of bistable switches, such as those including more PdP cycles, those with interactions between upstream PdP cycles, and those with feedback of non-target reactants; and (2) a detailed analysis of parameter sensitivity on the bistable region may help in the design of specific bistable switches with different response diagrams in synthetic biology.

In summary, our results emphasize the different and independent roles of cellular ATP levels (kinetics) and hydrolysis free energy (thermodynamics), as determined by the network structure. Some inefficient network structures in cell signaling pathways could be beneficial in maintaining biological functions against [ATP] and $\Delta\mu$ noise.

ACKNOWLEDGMENTS

The authors are grateful to Dr. H. Qian, Dr. H. Ge, Dr. H. Wang, and K. Kong for helpful discussions. This work was supported by the National Natural Science Foundation of China (Grants No. 12174007 and No. 12090054), the National Key Research and Development Program of China (Grants No. 2020YFA0906900 and No. 2018YFA0900200), and the Starry Night Science Fund of Zhejiang University Shanghai Institute for Advanced Study.

APPENDIX: THEORETICAL ANALYSIS OF BISTABLE REGION BORDERS IN THE SINGLE-PDP-CYCLE NETWORK WITH AUTOCATALYSIS

The single-PdP-cycle model with the autocatalysis of S_p by its dimer can be described by Eq. (5). The necessary conditions for saddle-node bifurcation [Eq. (8)] are written as

$$\begin{aligned} f(x,a,d) = \frac{dx}{dt} &= -(a+d)x^3 + ax^2 \\ &\quad - (p_1+p_2)x + p_2 = 0, \\ \frac{df}{dx} &= -3(a+d)x^2 + 2ax - (p_1+p_2) = 0. \end{aligned} \tag{A1}$$

By solving the two equations above, we figure out the relationship between $a \sim$ [ATP] and $d \sim$ [ADP] in Eqs. (A1), when the system meets the bifurcation condition (on the bistable region borders). Meanwhile, solving the two real root conditions of the cubic equation $f(x,a,d) = 0$ (discriminant formulas $\Delta = 0$) can easily derive the same relationships, where $\Delta = B^2C^2 - 4AC^3 - 4B^3D - 27A^2D^2 + 18ABCD$, $A = -(a+d)$, $B = a$, $C = -(p_1+p_2)$, and $D = p_2$.

The relationships $d = d_1(a)$ and $d = d_2(a)$ are formulated as below:

$$\begin{aligned} d_1(a) &= K(g_1(a) - 2\sqrt{g_2(a)}), \\ d_2(a) &= K(g_1(a) + 2\sqrt{g_2(a)}), \end{aligned} \tag{A2}$$

where

$$\begin{aligned} g_1(a) &= -2(p_1+p_2)^3 + \left[9(p_1+p_2)p_2 - 27p_2^2\right]a, \\ g_2(a) &= [(p_1+p_2)^2 - 3p_2a]^3, \quad \text{and} \quad K = \frac{1}{27p_2^2}. \end{aligned} \tag{A3}$$

First, since [ATP] and [ADP] are both positive ($a, d > 0$), the existence of the bistable region requires that the intersection point (a^*, d^*) of the two curves is in the first quadrant of $a - d$ space,

$$a^* = \frac{(p_1+p_2)^2}{3p_2} > 0, \tag{A4}$$

and

$$\begin{aligned} d^* = d_{1/2}(a^*) &= K(g_1(a^*) \mp 2\sqrt{g_2(a^*)}) \\ &= Kg_1(a^*) = K(p_1+p_2)^2(p_1 - 8p_2) > 0 \end{aligned} \tag{A5}$$

which means $p_1 > 8p_2$. Then we have the free-energy level,

$$\Delta\mu^*/(k_BT) = \ln(\gamma^*) = \ln\left(\frac{a^*p_1}{d^*p_2}\right) = \ln\left(\frac{9}{2(1-8p_2/p_1)}\right). \tag{A6}$$

Second, by solving the equations $d_1(a_1) = 0$ and $d_2(a_2) = 0$, we have the formula of the maximum relative width of bistable region [Eq. (11)], which is validated by simulation of random sampling (p_1, p_2) [Fig. 4(b)]. These two theoretical analysis infer that the forward reaction rate (p_1) of dephosphorylation reaction should be much larger than the backward one (p_2) to form a effective and robust bistable switch.

Third, we estimate the slope of bistable region borders (SLP) by functions $d(a)$:

$$\begin{aligned} \mathrm{SLP} = \frac{\partial\Delta\mu}{\partial a} &\sim \frac{1}{\gamma}\frac{\partial\gamma}{\partial a} = \frac{\partial}{\partial a}\left(\frac{ap_1}{dp_2}\right) \\ &= \frac{p_1}{p_2d^2}\left(d - a\frac{\partial d}{\partial a}\right). \end{aligned} \tag{A7}$$

Since p_1, p_2, and d are all positive, the value of above is uniquely dependent on the term inside brackets.

When $d(a) = d_2(a)$, it is straightforward to figure out that SLP < 0 [Eq. (A8)] with the condition $a < a^* = (p_1 + p_2)^2/3p_2$. When $d(a) = d_1(a)$, SLP can be formulated by Eq. (A9), where $y = 3a/[p_2(p_1/p_2 + 1)^2]$ is restricted by the same condition ($a < a^*$) and then belongs to $(0, 1)$. Since the $U(y)$ is a monotonic decreasing function, $\partial U(y)/\partial y = -3y/(2\sqrt{1-y}) < 0$, SLP for $d_1(a)$ is also negative. In addition, simulations are consistent with the analytical conclusion that two borders are both negative, as shown in Fig. 2.

$$d_2 - a\frac{\partial d_2}{\partial a} = \frac{p_2}{27}\left\{-2\left(\frac{p_1}{p_2}+1\right)^3 - \left[2\left(\frac{p_1}{p_2}+1\right)^2 + \frac{3a}{p_2}\right]\sqrt{\left(\frac{p_1}{p_2}+1\right)^2 - \frac{3a}{p_2}}\right\}$$
$$< \frac{p_2}{27}\left\{-2(8+1)^3 - \left[2(8+1)^2 + \frac{3a}{p_2}\right]\sqrt{(8+1)^2 - \frac{3a}{p_2}}\right\} < 0, \tag{A8}$$

$$d_1 - a\frac{\partial d_1}{\partial a} = \frac{p_2}{27}\left(\frac{p_1}{p_2}+1\right)^3\left\{-2 + \left[2 + \frac{3a/p_2}{(p_1/p_2+1)^2}\right]\sqrt{1 - \frac{3a/p_2}{(p_1/p_2+1)^2}}\right\}$$
$$= \frac{p_2}{27}\left(\frac{p_1}{p_2}+1\right)^3 U(y) < \frac{p_2}{27}\left(\frac{p_1}{p_2}+1\right)^3 U(y=0) = 0. \tag{A9}$$

[1] E. Schrödinger, *What Is Life? The Physical Aspect of the Living Cell* (The University Press, Cambridge, 1944).

[2] X. Fang, K. Kruse, T. Lu, and J. Wang, Nonequilibrium physics in biology, Rev. Mod. Phys. **91**, 045004 (2019).

[3] X. Yang, M. Heinemann, J. Howard, G. Huber, S. Iyer-Biswas, G. L. Treut, M. Lynch, K. L. Montooth, D. J. Needleman, S. Pigolotti, J. Rodenfels, P. Ronceray, S. Shankar, I. Tavassoly, S. Thutupalli, D. V. Titov, J. Wang, and P. J. Foster, Physical bioenergetics: Energy fluxes, budgets, and constraints in cells, Proc. Natl. Acad. Sci. USA **118**, e2026786118 (2021).

[4] J. J. Hopfield, Kinetic proofreading: A new mechanism for reducing errors in biosynthetic processes requiring high specificity, Proc. Natl. Acad. Sci. USA **71**, 4135 (1974).

[5] H. Qian and T. C. Reluga, Nonequilibrium thermodynamics and nonlinear kinetics in a cellular signaling switch, Phys. Rev. Lett. **94**, 028101 (2005).

[6] G. Lan, P. Sartori, S. Neumann, V. Sourjik, and Y. Tu, The energy-speed-accuracy trade-off in sensory adaptation, Nat. Phys. **8**, 422 (2012).

[7] Y. Cao, H. Wang, Qi Ouyang, and Y. Tu, The free-energy cost of accurate biochemical oscillations, Nat. Phys. **11**, 772 (2015).

[8] D. Zhang, Y. Cao, Q. Ouyang, and Y. Tu, Synchronization of coupled molecular oscillators, Nat. Phys. **16**, 95 (2020).

[9] C. C. Govern and P. R. Ten Wolde, Energy dissipation and noise correlations in biochemical sensing, Phys. Rev. Lett. **113**, 258102 (2014).

[10] S. Guan, L. Xu, Q. Zhang, and H. Shi, Trade-offs between effectiveness and cost in bifunctional enzyme circuit with concentration robustness, Phys. Rev. E **101**, 012409 (2020).

[11] J. A. Owen, T. R. Gingrich, and J. M. Horowitz, Universal thermodynamic bounds on nonequilibrium response with biochemical applications, Phys. Rev. X **10**, 011066 (2020).

[12] P. Sartori and S. Pigolotti, Thermodynamics of error correction, Phys. Rev. X **5**, 041039 (2015).

[13] U. Sathyanarayanan, M. Musa, P. Bou Dib, N. Raimundo, I. Milosevic, and A. Krisko, ATP hydrolysis by yeast Hsp104 determines protein aggregate dissolution and size in vivo, Nat. Commun. **11**, 1 (2020).

[14] M. Takaine, H. Imamura, and S. Yoshida, High and stable ATP levels prevent aberrant intracellular protein aggregation in yeast, eLife **11**, e67659 (2022).

[15] K. Xu, N. Yin, M. Peng, E. G. Stamatiades, A. Shyu, P. Li, X. Zhang, M. H. Do, Z. Wang, K. J. Capistrano, C. Chou, A. G. Levine, A. Y. Rudensky, and M. O. Li, Glycolysis fuels phosphoinositide 3-kinase signaling to bolster T cell immunity, Science **371**, 405 (2021).

[16] D. G. Nicholls, The pancreatic β-cell: A bioenergetic perspective, Physiol. Rev. **96**, 1385 (2016).

[17] P. Rorsman and F. M. Ashcroft, Pancreatic β-cell electrical activity and insulin secretion: Of mice and men, Physiol. Rev. **98**, 117 (2018).

[18] D. Zhao, T. Wang, J. Zhao, D. Li, Z. Lin, Z. Chen, Q. Ouyang, H. Qian, Y. V. Fu, and F. Li, Nonequilibrium and nonlinear kinetics as key determinants for bistability in fission yeast G2-M transition, arXiv:1610.09637 [q-bio.MN].

[19] H. Qian, Phosphorylation energy hypothesis: Open chemical systems and their biological functions, Annu. Rev. Phys. Chem. **58**, 113 (2007).

[20] J. E. Ferrell, J. R. Pomerening, S. Y. Kim, N. B. Trunnell, W. Xiong, C. Y. F. Huang, and E. M. Machleder, Simple, realistic models of complex biological processes: Positive feedback and bistability in a cell fate switch and a cell cycle oscillator, FEBS Lett. **583**, 3999 (2009).

[21] A. Verdugo, P. K. Vinod, J. J. Tyson, and B. Novak, Molecular mechanisms creating bistable switches at cell cycle transitions, Open Biol. **3**, 120179 (2013).

[22] S. Mochida, S. Rata, H. Hino, T. Nagai, and B. Novák, Two bistable switches govern M Phase entry, Curr. Biol. **26**, 3361 (2016).

[23] J. E. Ferrell, Jr. and E. M. Machleder, The biochemical basis of an all-or-none cell fate switch in xenopus oocytes, Science **280**, 895 (1998).

[24] C. P Bagowski, Jr. and J. E. Ferrell, Bistability in the JNK cascade, Curr. Biol. **11**, 1176 (2001).

[25] P. Zhou, X. Gao, X. Li, L. Li, C. Niu, Q. Ouyang, H. Lou, T. Li, and F. Li, Stochasticity triggers activation of the S-phase checkpoint pathway in budding yeast, Phys. Rev. X **11**, 011004 (2021).

[26] H. Ge and H. Qian, Thermodynamic limit of a nonequilibrium steady state: Maxwell-type construction for a bistable biochemical system, Phys. Rev. Lett. **103**, 148103 (2009).

[27] M. Vellela and H. Qian, Stochastic dynamics and non-equilibrium thermodynamics of a bistable chemical system: The Schlögl model revisited, J. R. Soc. Interface. **6**, 925 (2009).

[28] C. Jin, X. Yan, and F. Li, Non-equilibrium and stochasticity influence the activation process of the yeast DNA damage pathway, Sci. China Phys. Mech. Astron. **61**, 028721 (2018).

[29] A. Ehrmann, B. Nguyen, and U. Seifert, Interlinked GTPase cascades provide a motif for both robust switches and oscillators, J. R. Soc. Interface. **16**, 20190198 (2019).

[30] D. Morgan, *The Cell Cycle: Principles of Control*, 2nd. ed. (Oxford University Press, London, 2017).

[31] F. Schlögl, Chemical reaction models for non-equilibrium phase transitions, Z. Angew. Phys. **253**, 147 (1972).

[32] See Supplemental Material at http://link.aps.org/supplemental/10.1103/PhysRevResearch.6.033050 for details of mathematical models, analytical derivations and numerical results.

[33] Y. A. Kuznetsov, *Elements of Applied Bifurcation Theory* (Springer, New York, 2010).

[34] T. Finkel and P. M. Hwang, The Krebs cycle meets the cell cycle: Mitochondria and the G1-S transition, Proc. Natl. Acad. Sci. USA **106**, 11825 (2009).

[35] M. Tantama, J. Ramón Martínez-François, R. Mongeon, and G. Yellen, Imaging energy status in live cells with a fluorescent biosensor of the intracellular ATP-to-ADP ratio, Nat. Commun. **4**, 2550 (2013).

[36] M. Takaine, M. Ueno, K. Kitamura, H. Imamura, and S. Yoshida, Reliable imaging of ATP in living budding and fission yeast, J. Cell Sci. **132**, jcs230649 (2019).

[37] W.-H. Lin and C. Jacobs-Wagner, Connecting single-cell ATP dynamics to overflow metabolism, cell growth, and the cell cycle in *Escherichia coli*, Curr. Biol. **32**, 3911 (2022).

[38] Y. Sun, D. Li, C. Ni, Y. Ge, H. Qian, Q. Ouyang, and F. Li, ATP hydrolysis kinetics and thermodynamics as determinants of calcium oscillation in pancreatic β cells, Phys. Rev. Res. **4**, 043142 (2022).